1-1-2010

# Nanofluid-Based Direct Absorption Solar Collector

Todd Otanicar
*Loyola Marymount University*, totanicar@lmu.edu

P. E. Phelan

R. S. Prasher

G. Rosengarten

R. A. Taylor

# Nanofluid-based direct absorption solar collector

Todd P. Otanicar,[1,a)] Patrick E. Phelan,[2] Ravi S. Prasher,[2] Gary Rosengarten,[3] and Robert A. Taylor[2]
[1]*Department of Mechanical Engineering, Loyola Marymount University, Los Angeles, California 90045, USA*
[2]*School of Mechanical, Aerospace, Chemical and Materials Engineering, Arizona State University, Tempe, Arizona 85287, USA*
[3]*School of Mechanical and Manufacturing Engineering, University of New South Wales, Sydney, New South Wales 2052, Australia*

(Received 13 October 2009; accepted 23 April 2010; published online 26 May 2010)

Solar energy is one of the best sources of renewable energy with minimal environmental impact. Direct absorption solar collectors have been proposed for a variety of applications such as water heating; however the efficiency of these collectors is limited by the absorption properties of the working fluid, which is very poor for typical fluids used in solar collectors. It has been shown that mixing nanoparticles in a liquid (nanofluid) has a dramatic effect on the liquid thermophysical properties such as thermal conductivity. Nanoparticles also offer the potential of improving the radiative properties of liquids, leading to an increase in the efficiency of direct absorption solar collectors. Here we report on the experimental results on solar collectors based on nanofluids made from a variety of nanoparticles (carbon nanotubes, graphite, and silver). We demonstrate efficiency improvements of up to 5% in solar thermal collectors by utilizing nanofluids as the absorption mechanism. In addition the experimental data were compared with a numerical model of a solar collector with direct absorption nanofluids. The experimental and numerical results demonstrate an initial rapid increase in efficiency with volume fraction, followed by a leveling off in efficiency as volume fraction continues to increase. © *2010 American Institute of Physics.* [doi:10.1063/1.3429737]

## I. INTRODUCTION

Sustainable energy generation is one of the most important challenges facing society today. Solar energy offers a solution, with the hourly solar flux incident on the Earth's surface being greater than all of the human consumption of energy in a year.[1] The challenge lies in efficiently collecting and converting this energy into something useful. One of the principle methods of collection is through solar thermal collectors, which vary drastically in the amount of solar flux captured[2,3] as well as the method for capture.[4] The most common type of solar thermal collector utilizes a black surface as the absorber, which then transfers heat to a fluid running in tubes embedded within or fused onto the surface. In this case the efficiency is limited by not only how effective the absorber captures solar energy but also how effectively the heat is transferred to the working fluid. An approach that has been proposed to enhance the efficiency of collectors while simplifying the system is to directly absorb the solar energy within the fluid volume, the so-called direct absorption solar collector (DASC).[2]

The DASC was originally proposed in the 1970s as a simplification to solar thermal collector design and as a way to potentially enhance the efficiency by absorbing the energy with the fluid volume.[2,3,5,6] Typical fluids used in solar thermal collectors have been shown to have extremely low absorptive properties over the solar spectrum,[7] demonstrating the necessity of seeding the

a)Author to whom correspondence should be addressed. Electronic mail: totanicar@lmu.edu.

 

fluid with some sort of particle to enhance the absorption of the base fluid. For low flux collectors, used for hot water heating, this has been typically done with India Ink,[2] a suspension of micron-sized carbonaceous particles in shellac. For high flux collectors the particles, again micron-sized, are suspended in falling films or seeded in a high-velocity gas stream.[3,6] Traditional micron-sized seeding particles for DASCs suffer from particles settling out of solution, clogging of pumps and valves, fouling of transparent tubing,[2] and absorption spectrums dominated by the bulk material properties. Nanoparticles offer the potential of improving the radiative properties of liquids leading to an increase in the efficiency of DASCs. Additionally, it has been shown that mixing nanoparticles in a liquid (nanofluid) has a dramatic effect on the liquid thermophysical properties such as thermal conductivity.[8]

The impact of particles on the absorption of radiative energy has been of interest for many years for a variety of applications. More recently researchers have become interested in the radiative properties of nanoparticles in liquid suspensions especially for medical and other applications[9,10] due to the tunability of the absorption spectrum[11] and the large potential modifications to the effective optical properties of the system.[12] A recent theoretical study by two of the coauthors[13] showed that efficiency of low-temperature DASCs can be increased by using nanofluids as the fluidic medium. One of the unique benefits offered by the nanofluids is that when metallic nanoparticles are used, which are smaller than the mean free path of the material, the absorption spectrum is typically broadened[14] while maintaining a distinct absorption peak leading to a further enhancement in the absorption efficiency through the solar spectrum. This broadening allows the nanofluid to absorb a larger portion of the spectrum, but maintaining a peak can allow the user to tailor at which wavelength the absorption is maximized. Besides the benefits to the optical and radiative properties, nanofluids provide other benefits such as increased thermal conductivity[8] and particle stability over micron-sized suspensions, which provide potential improvements to the operating efficiency of a DASC.

## II. EXPERIMENTAL SETUP

The test apparatus was built around a micro-solar-thermal-collector that measures $3 \times 5$ cm$^2$, with a channel depth of 150 $\mu$m. The microchannel geometry was selected to minimize the amount of nanofluid needed for each collector test. Furthermore the depth of the channel allowed for the measurement of appreciable temperature gain for the pure fluid cases while allowing a large range of nanofluids to be tested where the expected amount of energy reaching the bottom of the channel would be nonzero. The collector glazing is a low-reflectance glass of thickness 3.3 mm for all experiments. Three different groups of nanofluids, with water as the base fluid, were considered: Graphite sphere-based (30 nm diameter, nominal), carbon nanotube-based (6–20 nm diameter, 1000–5000 nm length), and silver sphere-based (20 and 40 nm diameters). These fluids were either tested in varying volume fractions or varying particle sizes to understand how these variables impact solar thermal energy collection. Figure 1(a) shows the experimental collector schematic, while Fig. 1(b) demonstrates the uniformity of the temperature profile shortly after entering the collector. Figure 2 shows representative samples of nanofluids tested. The collector back surface was coated with a reflective aluminum tape for all experiments with nanofluids and one of the experiments with pure water. The reflectivity of the aluminum tape was measured in a spectrophotometer with an integrating sphere, although the tape was very smooth, and we assumed the reflectance to be specular. The collector was also tested with a matte black paint applied to the copper plate. The fluid depth was controlled with a metal spacer of thickness 150 $\mu$m. To simulate the solar spectrum a SuperPAR64 lamp was used at a height so that 1000 W/m$^2$ of radiative flux was measured incident on the collector. The spectrum of the lamp was measured at a color temperature of 3158 K, providing a decent approximation of the solar spectrum (note: The numerical model uses this adjusted color temperature to generate the irradiance spectrum). The collector was illuminated at normal irradiance in all experiments. The overall beam divergence was small over the small collector area. Three T-type thermocouples were mounted to measure the inlet and outlet temperatures of the fluid, plus a measurement of the copper plate temperature midway between the inlet and outlet ports. The whole system was

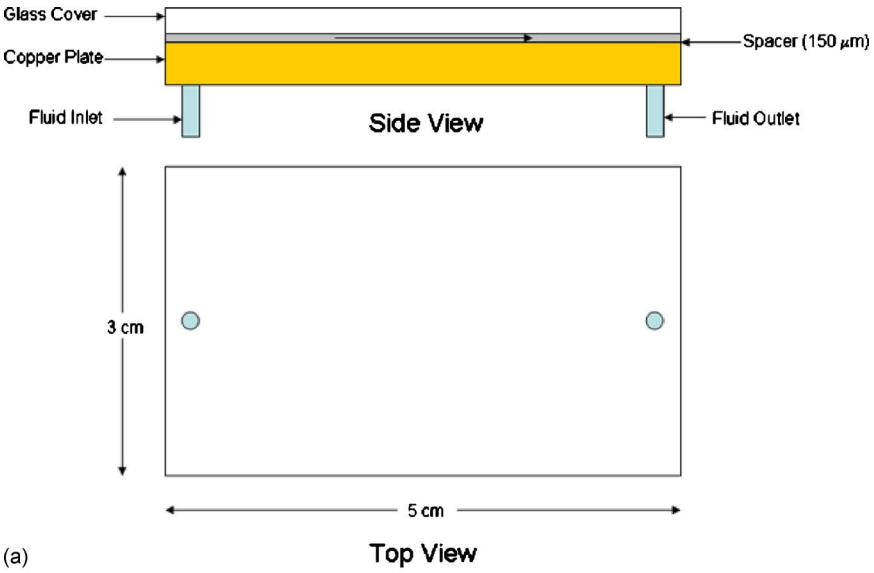


(a)

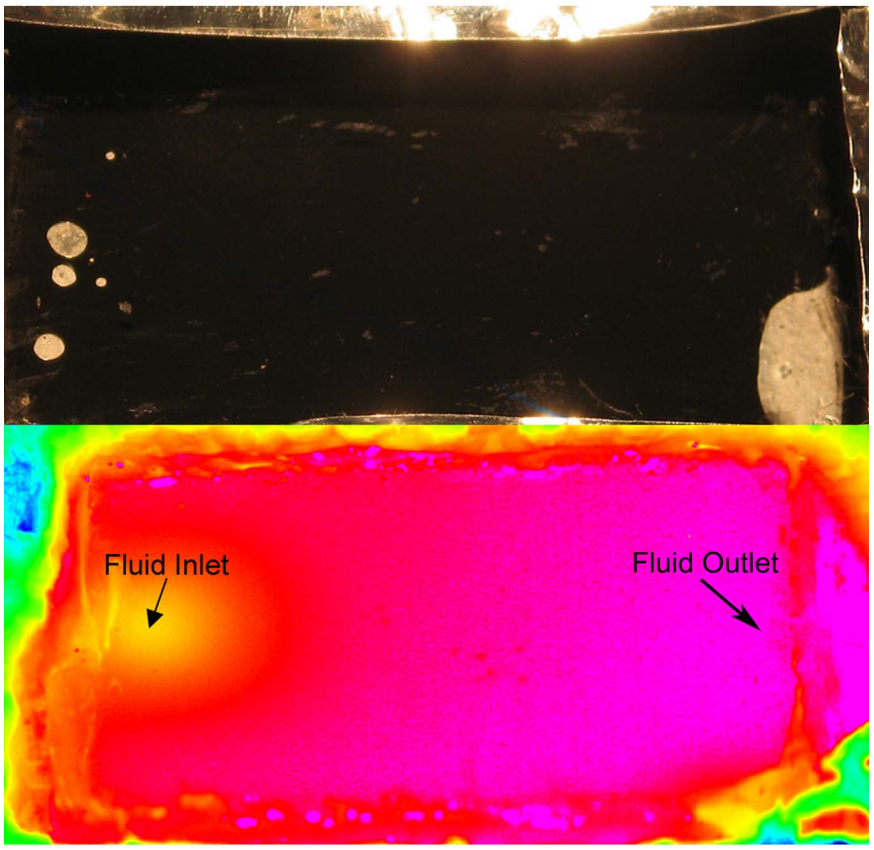


(b)

FIG. 1. Microsolar thermal collector. (a) Experimental schematic. (b) Infrared image demonstrating rapid temperature increase (blue: coolest; pink: warmest).

insulated within a Styrofoam block to limit heat loss from the back and sides of the collector. The Styrofoam block was shielded from incident radiation with aluminum so as to not absorb any of the simulated sunlight. The flow rate was controlled via a syringe pump and was set to 42 ml/h, chosen to allow measurable temperature rises for all the fluids tested. The nanofluids were pre-


FIG. 2. Representative nanofluid samples tested in microcollector.

pared by suspending various size, shape, and material nanoparticles in de-ionized water. To help minimize the effects of aggregation, the fluids were prepared with sodium dodecyl-sulfate surfactant of equal mass to the nanoparticles. All of the suspensions were sonicated for 30 min prior to use in the micro-solar-collector. Due to the sonication and use of surfactant, the nanofluids were often filled with air bubbles, which would become entrained in the collector channel; this required all the nanofluids to be degassed in a vacuum chamber prior to charging the collector with nanofluid. In addition the collector was taken apart and cleaned after every run with nanofluid to minimize particle buildup on the glass and back surface. Experimentally we focus on two parameters important to the operation of solar thermal collectors: The steady-state efficiency and the stagnation temperature (temperature at zero flow rate). The stagnation temperature difference is often used as a means to determine the overall heat loss of the physical system.

## III. NUMERICAL MODEL

### A. Comparison of volumetric- and surface-based absorptions

A simple model can be used to show the benefit of volumetric-based absorption over area-based absorption. Although previous studies indicate the benefit of such a system[2] from a collector efficiency standpoint, a simplified approach is used to determine the overall absorptance and reflectance for a volumetric and surface-based system. The reflectance from the system is approximated by applying the Maxwell–Garnett effective medium theory, valid for the independent scattering assumption, to obtain the effective optical properties of the nanofluid,[15]

$$\frac{\varepsilon_{\text{eff}}-\varepsilon_f}{\varepsilon_{\text{eff}}+2\varepsilon_f}=f_v\frac{\varepsilon_p-\varepsilon_f}{\varepsilon_p-2\varepsilon_f}, \tag{1}$$

where $\varepsilon_{\text{eff}}$ is the effective dielectric constant of the nanofluid, $\varepsilon_p$ is the dielectric constant of the nanoparticles, $\varepsilon_f$ is the dielectric constant of the base fluid, and $f_v$ is the volume fraction. These optical properties are then used to calculate the reflectance at normal incidence at the air-fluid interface using the Fresnel relations,[15]

$$R=\frac{(n_{\text{eff}}-n_{\text{air}})^2+(k_{\text{eff}}-k_{\text{air}})^2}{(n_{\text{eff}}+n_{\text{air}})^2+(k_{\text{eff}}+k_{\text{air}})^2}, \tag{2}$$

where $R$ is the reflectance, $n_{\text{eff}}$ is the effective refractive index of the nanofluid, $k_{\text{eff}}$ is the effective extinction index of the nanofluid, $n_{\text{air}}$ is the refractive index of air, and $k_{\text{air}}$ is the extinction index of air (normally equal to zero). The absorbed energy is then found by solving a simplified version

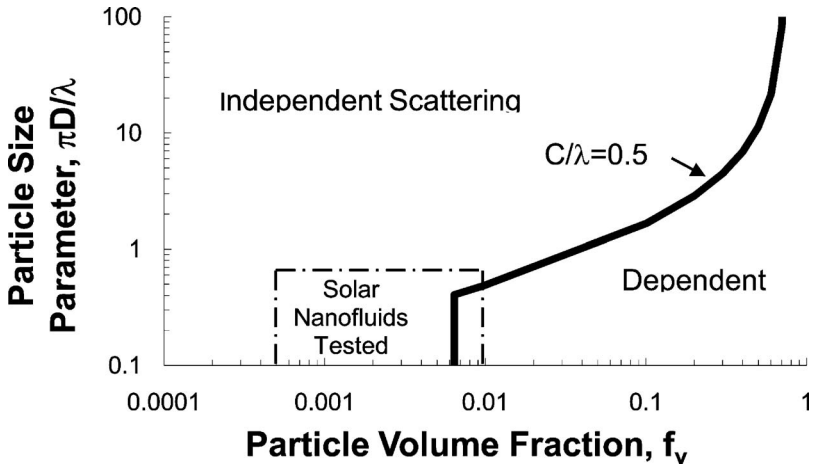


FIG. 3. Scattering regime map (Ref. 16).

of the RTE, omitting the blackbody emission term, and comparing the incoming energy to the absorbed energy,

$$\frac{dI_\lambda}{dy} = -\sigma_{e,\lambda} I_\lambda \tag{3}$$

where $I$ is the incoming radiation after subtracting the reflected component, $\lambda$ is the wavelength, and $\sigma_e$ is the extinction coefficient. To find the extinction coefficient, the approximation of independent scattering, which greatly simplifies the analysis of the scattering problem, is used and can be justified with the use of the classical scattering map developed by Brewster and Tien[16] shown in Fig. 3 including the region for the fluids tested. Based on the independent scattering assumption and the approximation of Rayleigh scattering (size parameter $\alpha = \pi D/\lambda \ll 1$), the following relations for the scattering and absorption efficiency of a spherical particle are used in the model:[4]

$$Q_{s,\lambda} = \frac{8}{3}\alpha^4 \left| \frac{m^2 - 1}{m^2 + 2} \right|^2, \tag{4}$$

$$Q_{a,\lambda} = 4\alpha \, \mathrm{Im}\left\{ \frac{m^2 - 1}{m^2 + 2} \right\}, \tag{5}$$

where $m$ is the relative complex refractive index of the particles to the fluid, assuming the fluid is nonabsorbing. The absorption and scattering efficiencies are used to determine the extinction coefficient,[15]

$$\sigma_{e,\lambda} = \frac{3 f_v (Q_{s,\lambda} + Q_{a,\lambda})}{2D}. \tag{6}$$

For the surface absorber system, Eq. (2) is utilized instead to find the reflectance of the surface metal and the air interface where the effective optical properties are replaced by the bulk material properties. The absorptance of the surface is then simply 1 minus the reflectance. This simple method allows for a quick comparison between volumetric and surface absorptions.

### B. Numerical modeling of DASC

The work of Tyagi *et al.*[13] laid the groundwork for a numerical model of a direct absorption receiver that utilizes nanofluids. Much of this work is based on models that solve the radiative

transport equation (RTE) coupled to the energy equation for small particles suspended in a gas.[17] The RTE is used in this model to include the emission term in addition to the previous model, which only used the extinction coefficient,

$$\frac{dI_{i,\lambda}}{dy} = \sigma_{a,\lambda} I_{b,\lambda}[T(y)] - \sigma_{e,\lambda} I_{i,\lambda} \tag{7}$$

where $\sigma_{a,\lambda}$ is the spectral absorption coefficient. The subscript $i$ is used to represent the directional nature of the intensity, +1 representing the direction of the solar radiation and $-1$ in the opposite direction of the incoming solar radiation. The in-scattering term is neglected in the RTE due to its complexity and the fact that the scattering coefficient is extremely small in comparison to the absorption coefficient in the Rayleigh regime. It should be noted that the effects of the surfactant are not modeled in the current system but are expected to be extremely small in relation to the extremely large extinction coefficients created by the nanoparticles and therefore not significant. The boundary conditions outlined by Kumar and Tien[17] are specified in Eqs. (8) and (9),

$$I_{-1,\lambda}(L) = \varepsilon_{w,\lambda} I_{b,\lambda}[T(L)] + \rho_{w,\lambda} I_{+,\lambda}, \tag{8}$$

$$I_{+1,\lambda}(0) = S_\lambda(1 - \rho_{g,\lambda} - \alpha_{g,\lambda}) + \rho_{g,\lambda} I_{-1,\lambda}(0) + \alpha_{g,\lambda} I_{b,\lambda}[T(0)], \tag{9}$$

where $\varepsilon_{w,\lambda}$ is the spectral wall emittance, $\rho_{w,\lambda}$ is the spectral wall reflectance, $\rho_{g,\lambda}$ is the spectral glass reflectance, $\alpha_{g,\lambda}$ is the spectral glass absorptance, and $S_\lambda$ is the incident spectral radiation on the top layer of the fluid. The inclusion of the glass absorptance in Eq. (9) is especially important in modeling the experimental setup since the color temperature of the light shifts the wavelength of peak intensity in the spectral direction where glass is more absorbing. The spectral properties of the incoming light and the emitted radiation can be determined with the blackbody relation given in Eq. (10),

$$I_\lambda(T) = \frac{2hc_0^2}{\lambda^5 \left[ \exp\left( \frac{hc_0}{\lambda k_B T} \right) - 1 \right]}, \tag{10}$$

where $h$ is Planck's constant, $k_B$ is the Boltzmann constant, and $c_0$ is the speed of light in a vacuum. The intensities are coupled with a two-dimensional steady-state energy equation to solve for the temperature profile within the fluid,

$$k\frac{\partial^2 T}{\partial y^2} - \frac{\partial q_r}{\partial y} = \rho c_p U \frac{\partial T}{\partial x}, \tag{11}$$

where $\rho$ is the fluid density, $k$ is the thermal conductivity, $c_p$ is the specific heat, and $U$ is the velocity. The velocity profile in this case is assumed to be independent of $x$ and $y$, a uniform velocity profile, for simplicity. The energy equation is coupled to the RTE through the divergence of the radiative flux,[17]

$$\frac{\partial q_r}{\partial y} = 2\int_\lambda \sigma_{a,\lambda} I_{b,\lambda}[T(y)] d\lambda - \int_\lambda \sigma_{a,\lambda} I_{-1,\lambda} d\lambda - \int_\lambda \sigma_{a,\lambda} I_{+1,\lambda} d\lambda. \tag{12}$$

The boundary conditions for the inlet and the base of the collector are as follows:

$$x = 0, \quad 0 < y < L, \quad T(0,y) = T_{\text{inlet}},$$
$$y = L, \quad x > 0, \quad q_r(L) - k \left.\frac{\partial T}{\partial y}\right|_{y=L} = 0, \tag{13}$$

where $y=L$ corresponds to the bottom of the fluid and $y=0$ corresponds to the top of the fluid (and the glass-fluid interface). The boundary condition for the top surface is combined convection and radiation,

$$y = 0, \quad x > 0, \quad h[T_\infty - T(x,0)] = -k \left.\frac{\partial T(x,y)}{\partial y}\right|_{y=0}, \tag{14}$$

where $h$ is the combined convection and radiation heat transfer coefficient experimentally determined from the stagnation temperature data.

### C. Overall model heat transfer coefficient

One factor that affects the prediction accuracy of the model is the overall heat transfer coefficient. A method to get an estimate of the overall heat transfer coefficient is to utilize the stagnation temperature and steady-state collector temperature at zero flow rate, by taking the ratio of the incoming absorbed solar energy to the difference of the stagnation temperature and ambient temperature. The stagnation temperature can be used to determine the loss coefficient, the overall heat transfer coefficient for the collector system,[18]

$$U_L = h = \frac{G}{T_s - T_{\text{amb}}}, \tag{15}$$

where $G$ is the absorbed solar radiation, $T_s$ is the stagnation temperature, and $T_{\text{amb}}$ is the ambient temperature. For the collector system tested the loss coefficients ranged from 23–34 W $\text{m}^{-2}$ $^\circ\text{C}^{-1}$ for all fluids and backing surfaces tested.

### D. Inclusion of size effects

In addition to the basic modeling that utilizes the bulk material properties and independent scattering assumption, we modified the model to include the impact of size-dependent effects on the nanoparticle optical properties. This modification is implemented in the numerical procedure by causing a modification to the extinction and absorption coefficients in the RTE. As the nanoparticle dimension decreases below the mean free path of the bulk material the optical properties are modified due to the interaction of the oscillation with the boundary. This effect has been modeled numerically[14,19] and confirmed experimentally[19] for nanoparticles. The optical properties for metals can be theoretically modeled with the Drude (free-electron) model as shown below,[14]

$$\varepsilon(\omega) = 1 - \frac{\omega_p^2}{\omega^2 - i\Gamma\omega}, \tag{16}$$

where $\omega_p$ is the plasmon frequency, $\omega$ is the frequency of the electromagnetic wave, and $\Gamma$ is the damping coefficient.[14] As the particle size is reduced below the mean free path of the material the oscillations of the free electrons begin to interact with the particle boundary; this effect results in a modification to the damping coefficient due to surface scattering.[14] The modification is then

$$\Gamma(D) = \Gamma_\infty + g\frac{v_f}{D}, \tag{17}$$

where $\Gamma_\infty$ is the bulk metal damping coefficient, $g$ is the proportionality factor (set to 1 for most cases[14]), $v_f$ is the Fermi velocity, and $D$ is the particle diameter. This modification can be coupled

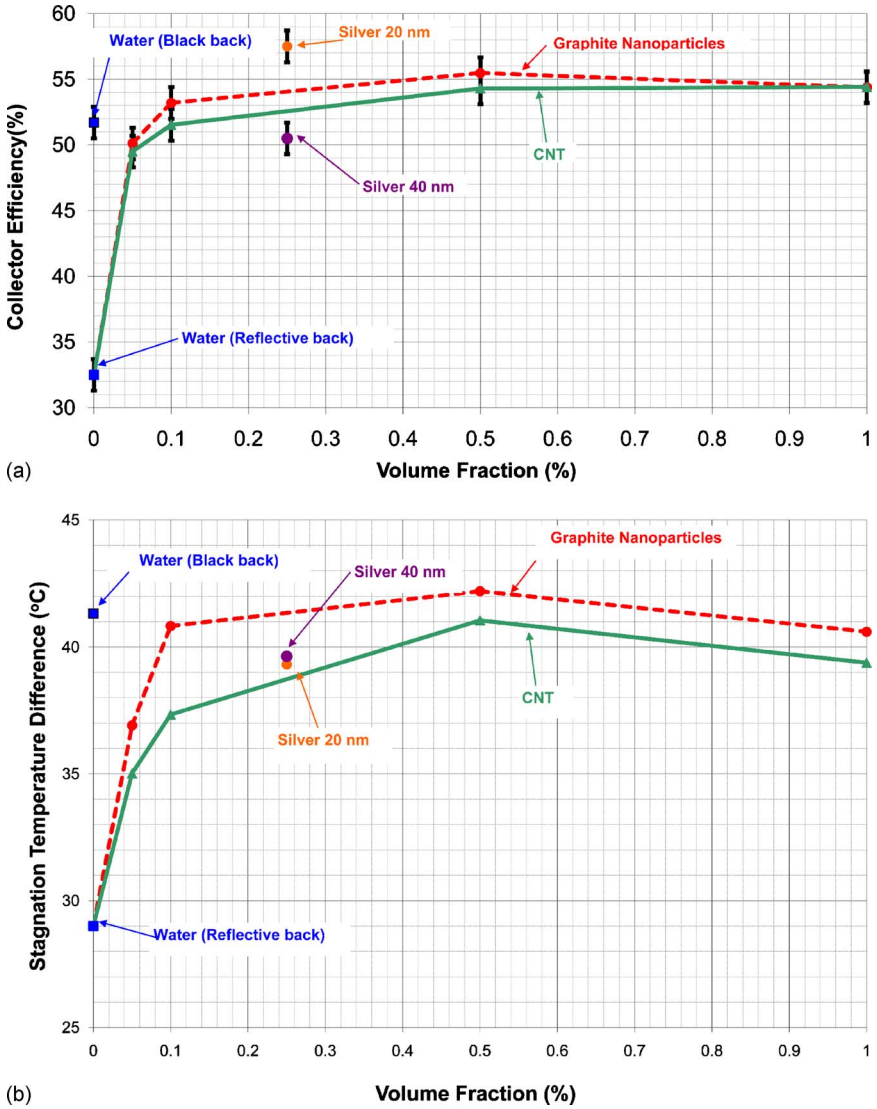


FIG. 4. Experimental microsolar thermal collector testing results. (a) Steady-state collector efficiency and (b) stagnation temperature difference as function of volume fraction.

with the bulk optical property data, which also include the effect of interband absorption[14] to yield a size-dependent complex dielectric function,

$$\varepsilon(\omega,D)=\varepsilon_{\text{bulk}}(\omega)+\omega_p^2\left(\frac{1}{\omega^2+\Gamma_\infty^2}-\frac{1}{\omega^2+\Gamma(D)^2}\right)+i\frac{\omega_p^2}{\omega}\left(\frac{\Gamma(D)}{\omega^2+\Gamma(D)^2}-\frac{\Gamma_\infty}{\omega^2+\Gamma_\infty^2}\right). \tag{18}$$

Overall, we modified the numerical model by Tyagi *et al.*[13] to account for the heat loss in our solar collector and the impact of particle size that appears in the absorption and scattering efficiency, as well as the modification of the bulk optical properties when the particle size is below the mean free path.[14]

## IV. RESULTS AND DISCUSSION

Figure 4(a) shows the experimental efficiency, which is the ratio of the usable thermal energy

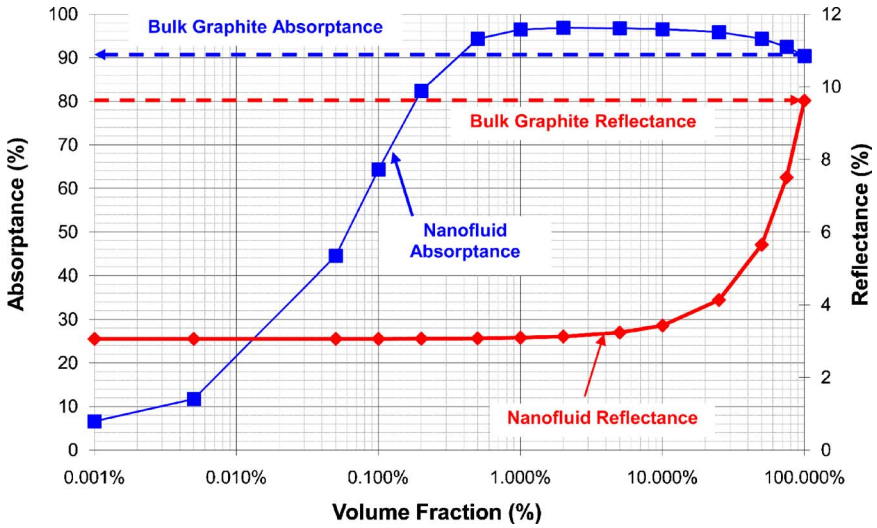


FIG. 5. Theoretical benefit of volumetric absorption when utilizing a 30 nm graphite nanofluid in comparison to conventional area-based absorption.

to the incident solar energy as defined below,[18] of the micro-solar-collector as a function of the nanoparticle volume fraction,

$$\eta = \frac{\dot{m} c_p (T_{\text{outlet}} - T_{\text{inlet}})}{G_T A}, \tag{19}$$

where $\dot{m}$ is the mass flow rate, $c_p$ is the specific heat of the fluid, $T_{\text{outlet}}$ is the collector outlet fluid temperature, $T_{\text{inlet}}$ is the inlet fluid temperature, $G_T$ is the solar irradiance, and $A$ is the collector area. The DASC data are compared to a conventional collector configuration where the solar energy is absorbed on a black plate surface. The addition of small amounts of nanoparticles results in a rapid enhancement in the efficiency from the pure fluid case until a volume fraction of approximately 0.5%. For 30 nm graphite nanoparticles, a maximum improvement, over a conventional flat surface absorber, of 3% can be achieved. With 20 nm silver particles an efficiency improvement of 5% can be achieved, while only a small difference ($\sim$1%) is observed between the CNT and the graphite spheres. After a volume fraction of 0.5%, the efficiency begins to level off and even decrease slightly with increasing volume fraction. One would expect this result since at low particle loadings, the transmittance of water is approached and thus little heating occurs, while at high particle loadings, the fluid absorption is very high. The most drastic difference in the steady-state efficiency between nanofluids is found for silver particles between 20 and 40 nm, where a 6% efficiency increase is observed when the particle size is halved. In addition Fig. 4(b) demonstrates a similar pattern for the stagnation temperature difference. Again a rapid increase is seen with the addition of nanoparticles, but this time a consistent maximum level is achieved, within 2 °C, but interestingly the differently-sized silver nanoparticles exhibit the same stagnation temperature difference.

By comparing the amount of solar energy absorbed and reflected by a fixed depth of nanofluid versus utilizing the same material but as a surface absorber, the benefit of volumetric absorption can be demonstrated with a simple numerical model. Figure 5 demonstrates that a volumetric-based absorption is a stronger absorber, as well as having reduced reflectance, over a surface-based system made from the same material. The results of the numerical model, which includes size effects as well as the overall heat loss coefficient determined experimentally, in comparison to the experimental results for 30 nm graphite nanoparticles, are shown in Fig. 6. The numerical model is shown to be accurate to within 5% of the experimental results across a wide range of volume fractions.

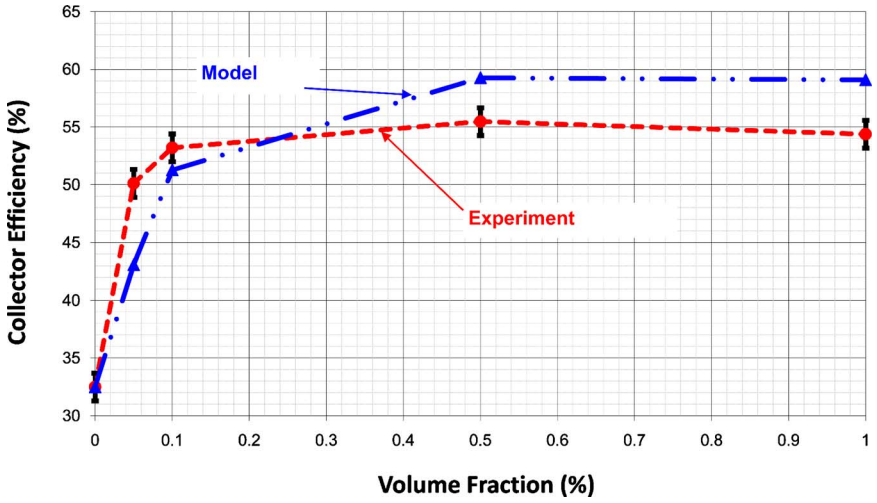


FIG. 6. Comparison of modeling and experimental results for 30 nm graphite spheres.

The efficiency and stagnation temperature behavior can be described by three effects created by adding nanoparticles to the fluid mixture in conjunction with the coupling to direct solar flux as follows: Drastic modification of the optical properties of the fluid, peak temperatures away from surfaces losing heat to ambient, and thermal conductivity enhancement. The first effect is the most obvious contributor to the rapid increase in efficiency as the addition of a small amount of particles to the fluid makes the clear fluid (water) completely opaque to the naked eye. One advantage of utilizing nanoparticles, instead of larger size particles, is much larger absorption efficiency in comparison to the scattering efficiency.[14] The most surprising result from the experimental work is the high efficiency level achieved with the 20 nm silver nanoparticles. The model does provide a qualitatively correct answer when including these impacts for the silver nanoparticles, showing a small increase (~2%) when the size is decreased from 40 to 20 nm diameter, as shown in Fig. 7. This figure also shows that reducing the particle size further leads to an even

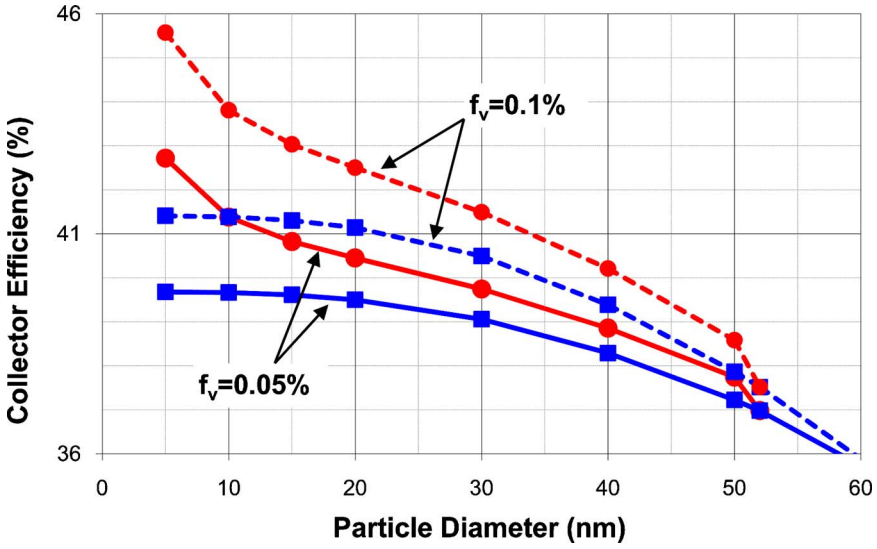


FIG. 7. Collector efficiency as a function of silver nanoparticle diameter (squares: bulk properties; circles: size-dependent properties) and volume fraction.

greater enhancement in efficiency through the dependence of the optical properties on particle size.

The effect of modifying the optical properties is obviously important in maximizing the amount of solar absorption, but it is also important in this style collector to try to distribute the amount of solar energy absorbed as evenly as possible within the fluid volume. This leads to a more uniform temperature profile, which limits the amount of heat loss at the boundaries as well as simplifies the design by eliminating a surface operating at extreme temperatures. Therefore the optimal collector design is one in which the peak temperature is located away from surfaces exposed to ambient temperatures; ideally this would be near the center of the fluid.

The benefit from modifying the bulk optical properties, the part caused by broadening the absorption peak as particle sized is decreased,[15] and the temperature profile explains the largest portions of the efficiency increase. We believe that part of the remaining increase is due to the enhancement in the thermal conductivity from the suspension of nanoparticles, which has been shown to increase with decreasing particle size,[8] and would also explain the lack of difference in stagnation temperatures between the silver nanofluids. Our model has confirmed that a small increase, less than 0.5%, can be achieved with reasonable increases in thermal conductivity for nanofluids.[8] These three effects acting together are what lead to the overall increase in collector efficiency observed.

## V. CONCLUSIONS

Using nanofluids as a DASC has been demonstrated here to offer unique advantages over conventional collectors: (1) Heating within the fluid volume, limiting the need for a hot surface, which only transfers heat to a small area of fluid, and allowing the peak temperature to be located away from surfaces losing heat to the environment; (2) variability of the size, shape, material, and volume fraction of the nanoparticles allows for tuning to maximize spectral absorption of solar energy throughout the fluid volume; (3) enhancement in the thermal conductivity can lead to efficiency improvements, although small, via more effective fluid heat transfer; and, finally, (4) vast enhancements in surface area due to the extremely small particle size, which makes nanofluid-based solar systems attractive for thermochemical and photocatalytic processes. For example, in the current geometry 30 nm diameter particles at 1% volume fraction have 300 times more surface area than the bottom of the channel itself. Further improvements to the efficiency could be achieved by taking advantage of particle size and shape distributions to make the volumetric absorber more selective. In addition by determining the optimum profile of volumetric absorption, potentially such that the maximum temperature is closer to the center of the fluid, one could minimize heat loss and further enhance the efficiency.

## ACKNOWLEDGMENTS

This material is based on the work supported by the National Science Foundation under Grant Nos. 0812778 (an East Asia and Pacific Summer Institutes fellowship) and 0932720. Any opinions, findings, and conclusions or recommendations expressed in this material are those of the author(s) and do not necessarily reflect the views of the National Science Foundation.

## NOMENCLATURE

| | |
|---|---|
| $A$ | Area [$m^2$] |
| $c_0$ | Speed of light [$m\ s^{-1}$] |
| $c_p$ | Specific heat [$J\ kg^{-1}\ K^{-1}$] |
| $D$ | Particle diameter [m] |
| $f_v$ | Volume fraction |
| $G$ | Incident solar radiation [$W\ m^{-2}$] |
| $h$ | Planck's constant [J s] |
| $h$ | Heat transfer coefficient [$W\ m^{-2}\ K^{-1}$] |
| $I$ | Spectral power [$W\ m^{-2}\ \mu m^{-1}$] |

| | |
|---|---|
| $k$ | Thermal conductivity [W $m^{-1}$ $K^{-1}$] |
| $k_B$ | Boltzmann Constant [J $K^{-1}$] |
| $L$ | Pathlength [m] |
| $\dot{m}$ | Mass flow rate [kg $s^{-1}$] |
| $N$ | Index of refraction |
| $q_r$ | Radiative flux [W $m^{-2}$] |
| $Q$ | Scattering or absorption efficiency |
| $R$ | Reflectance [%] |
| $S$ | Incoming solar radiation [W $m^{-2}$ $\mu m^{-1}$] |
| $T$ | Temperature [K] |
| $U$ | Velocity [m $s^{-1}$] |
| $U_L$ | Collector loss coefficient [W $m^{-2}$ $K^{-1}$] |
| $v_f$ | Fermi velocity [m $s^{-1}$] |
| $x, y$ | Coordinates |

## Greek Symbols

| | |
|---|---|
| $\Gamma$ | Damping coefficient |
| $\alpha$ | Particle size parameter |
| $\alpha$ | Absorptance |
| $\varepsilon$ | Emittance |
| $\varepsilon$ | Dielectric constant |
| $\rho$ | Reflectance |
| $\rho$ | Density [kg $m^{-3}$] |
| $\eta$ | Efficiency |
| $\sigma$ | Radiative coefficient [$m^{-1}$] |
| $\omega$ | Frequency [rad $s^{-1}$] |
| $\lambda$ | Wavelength [m] |

## Subscripts

| | |
|---|---|
| $a$ | Absorption |
| amb | Ambient |
| $b$ | Blackbody |
| $e$ | Extinction |
| eff | Effective |
| $f$ | Fluid |
| $f$ | Independent |
| $i$ | Directional |
| in | Collector inlet |
| out | Collector outlet |
| $P$ | Particle |
| $s$ | Stagnation |
| $w$ | Wall |
| $\infty$ | Bulk |
| $\lambda$ | Spectral |

[1] N. S. Lewis, Science **315**, 798 (2007).
[2] J. E. Minardi and H. N. Chuang, Sol. Energy **17**, 179 (1975).
[3] R. Bertocchi, J. Karni, and A. Kribus, Energy **29**, 687 (2004).
[4] S. A. Kalogirou, Prog. Energy Combust. Sci. **30**, 231 (2004).
[5] N. Arai, N. Itaya, and M. Hasatani, Sol. Energy **32**, 49 (1984).
[6] A. J. Hunt, "Small particle heat exchangers," Lawrence Berkeley Laboratory LBL-7841, 1978.
[7] T. P. Otanicar, P. E. Phelan, and J. S. Golden, Sol. Energy **83**, 969 (2009).
[8] X. Q. Wang and A. S. Majumdar, Int. J. Therm. Sci. **46**, 1 (2007).
[9] L. R. Hirsch, R. J. Stafford, J. A. Bankson, S. R. Sershen, B. Rivera, R. E. Price, J. D. Hazle, N. J. Halas, and J. L. West, Proc. Natl. Acad. Sci. U.S.A. **100**, 13549 (2003).
[10] G. L. Liu, J. Kim, Y. Lu, and L. P. Lee, Nature Mater. **5**, 27 (2006).
[11] N. Harris, M. J. Ford, and M. B. Cortie, J. Phys. Chem. B **110**, 10701 (2006).

[12] R. S. Prasher, J. Appl. Phys. **102**, 074316 (2007).
[13] H. Tyagi, P. E. Phelan, and R. S. Prasher, J. Sol. Energy Eng. **131**, 041004 (2009).
[14] U. Kreibig and V. Vollmer, *Optical Properties of Metal Clusters* (Springer, Berlin, 1998).
[15] C. F. Bohren and D. R. Huffman, *Absorption and Scattering of Light by Small Particles* (Wiley, New York, 1998).
[16] M. Q. Brewster and C. L. Tien, J. Heat Transfer **104**, 573 (1982).
[17] S. Kumar and C. L. Tien, Heat Transfer Phenomena in Radiation, Combustion and Fires, National Heat Transfer Conference, 1989.
[18] J. A. Duffie and W. A. Beckman, *Solar Engineering of Thermal Processes* (Wiley, New York, 1988).
[19] S. L. Westcott, J. B. Jackson, C. Radloff, and N. Halas, Phys. Rev. B **66**, 155431 (2002).